Front. Chem. Sci. Eng. 2021, 15(4): 998–1007
https://doi.org/10.1007/s11705-020-1994-x

RESEARCH ARTICLE

Highly uniform Ni particles with phosphorus and adjacent defects catalyze 1,5-dinitronaphthalene hydrogenation with excellent catalytic performance

Wei Xiong[1,2], Susu Zhou[1], Zeyong Zhao[1], Fang Hao (✉)[1], Zhihui Cai[1], Pingle Liu (✉)[1], Hailiang Zhang[2], Hean Luo[1]

1 College of Chemical Engineering, National & Local United Engineering Research Centre for Chemical Process Simulation and Intensification, Xiangtan University, Xiangtan 411105, China
2 College of Chemistry, Xiangtan University, Xiangtan 411105, China

Abstract This work proposes a modified activated carbon support, with defects and heteroatoms (N,P-ACs) by nitrogen and phosphorus doping to load non-noble nickel to catalyze aromatic compound hydrogenation. The Ni/N,P-ACs-900 (prepared at 900 °C) showed promising catalytic activity in liquid-phase 1,5-dinitronaphthalene hydrogenation with a 1,5-diaminonaphthalene yield of 95.8% under the mild condition of 100 °C, which is comparable to the commercial Pd/C catalyst. The nitrogen species were burned off at 900 °C, causing more defects for nickel metal loading, facilitating the interaction between the supports and the nickel metal, and resulting in highly dispersed metal particles. The computational study of the nickel binding energy has been conducted using density functional theory. It exhibits that the defects formed by heteroatom doping are beneficial to nickel anchoring and deposition to form highly uniform nickel particles. The phosphorus species in combination with the defects are suitable for H_2 adsorption and dissociation. These results reveal that the heteroatomic doping on the active carbon shows significant effects in the hydrogenation of the liquid-phase aromatic compounds. These findings could provide a promising route for the rational design of aromatic compound hydrogenation catalysts to significantly decrease the cost by instead using noble metal catalysts in the industry.

Keywords nitrogen and phosphorus doping, non-noble nickel catalyst, aromatic compounds hydrogenation

Received April 27, 2020; accepted July 22, 2020

E-mails: haofang.happy@163.com (Hao F);
liupingle@xtu.edu.cn (Liu P)

1 Introduction

Polycyclic aromatic amines (PAAs) are a kind of very important organic chemical, which have great economic value and are in great demand in industrial application [1]. Among them, 1,5-diaminonaphthalene has the highest value for producing 1,5-naphthalene diisocyanate (NDI), which is an important precursor in the synthesis of superior polyurethane. NDI polyurethane exhibits excellent physical properties due to the symmetry, regularity, and rigidity of the NDI molecules. It can also be applied in high temperature, high grease, and high mechanical wear conditions in the automotive, textile, machinery, petroleum, military, and printing industries [2,3]. In the industry process, catalytic hydrogenation is one of the most commonly used methods for the production of 1,5-diaminonaphthalene. The wide application of the noble metal catalysts, such as Pt/C and Pd/C, results in the high cost of the amines production. Therefore, non-noble metal catalysts have obtained an increasing amount of attention in the hydrogenation processes [4,5], and the cheap activated carbon is usually chosen to be the support material for its large surface area and price. However, the catalyst prepared directly from the activated carbon loaded non-noble metal catalysts always shows low catalytic activity.

Recently, heteroatomic doping has been considered as a feasible approach to tune the physical and chemical properties of carbon materials. It could also significantly improve the interaction between the support and the metal particles [6]. The heteroatom (N, P, B, O, and S) doping on the activated carbon can significantly improve the performance of activated carbon as a catalytic solid support [7–9]. It has been widely applied in gas adsorption

[10,11], oxygen reduction reaction [12,13], catalytic reaction [14–16], fuel cells [17,18], and electrochemical supercapacitors [19,20]. Among many dopant attempts within carbon materials, nitrogen has attracted significant attention. The nitrogen atom has been demonstrated as an electron-donating group to increase the electron density and adjust the physical and chemical properties of carbon materials [21,22]. Additionally, it could also facilitate catalytic performance by enhancing the adsorption of active metal elements, improving the dispersion, and affecting the valence of the active metal [23–26]. However, the nitrogen species is easily lost as the treatment temperature increases [27,28]. Phosphorus has similar properties as nitrogen for containing the same valance electrons. Furthermore, phosphorus presents stronger n-type behavior and electron-donating ability than nitrogen. The co-doping of nitrogen and phosphorus in the structure of carbon materials is promising to tune the chemical and physical properties of the carbon material, possibly resulting in better metal deposition condition and catalytic activity [29,30].

Herein, a commercially inexpensive coconut shell activated carbon is selected to co-dope with nitrogen and phosphorus by using 1-butyl-3-methylimidazolium dihydrogen phosphate (IL) as the dopant. The treated temperatures have also been investigated. These prepared nitrogen-phosphorus co-doped activated carbons (N,P-ACs) were employed as the support for preparing the non-noble nickel based hydrogenation catalyst. It shows that it could obtain highly-dispersed nickel particles as the treated temperature reached 900 °C. These catalysts showed attractive catalytic activity in the liquid phase hydrogenation of 1,5-dinitronaphthalene. The N,P-ACs pretreated at 900 °C loaded nickel catalyst (Ni/N,P-AC-900) performed decent activity and selectivity in the synthesis of 1,5-diaminonaphthalene. The density functional theory (DFT) calculation of the nickel binding energy has also been studied. It exhibited that co-doping nitrogen and phosphorus show a synergistic effect in this liquid-phase aromatic compound hydrogenation reaction. The present results are very encouraging and show the strong possibility of replacing noble catalysts by non-noble nickel catalysts in the aromatic hydrogenation industry to reduce the usage of rare precious metals and reduce catalytic cost.

2 Experimental

2.1 Materials

The activated carbon of a coconut shell was bought from Fujian Xinsen Carbon Co. Ltd., China. 1,5-dinitronaphthalene (97 wt-%) was supplied by Shanghai Jingchun Reagent Co. Ltd. Nickel nitrate ($Ni(NO_3)_2 \cdot 6H_2O$) was obtained from Shanghai Aibi Chemistry Reagent Co. Ltd. Commercial 5% Pd/C was bought from Shanghai Macklin Biochemical Co. Ltd. 1-butyl-3-methylimidazolium dihydrogen phosphate was purchased from Shanghai Cheng Jie Chemical Co. Ltd. 1,5-diaminonaphthalene (97 wt-%) was purchased from Alfa Aesar-A Johnson Matthey Company. All the other reagents were of analytical grade.

2.2 Catalyst preparation

The N,P-ACs were synthesized by an impregnation and subsequent annealing treatment, in which the coconut shell activated carbon was used as the carbon source, and IL was used as the nitrogen and phosphorus source. Specifically, the coconut shell activated carbon was added into an IL solution and then constantly stirred at 30 °C for 10 h. The impregnation solution was dried at 100 °C for 10 h and labeled as N,P-AC. Then, the activated carbon precursors were calcined in a tubular furnace under a nitrogen atmosphere at the targeted temperature for 2 h, in which the rate of heating was 3 $°C \cdot min^{-1}$ and the nitrogen flow rate was 50 $mL \cdot min^{-1}$, to obtain the N,P-AC supports. The active carbon pretreated by dopant were marked as N,P-AC-T (T = 800 °C and 900 °C), where T is the temperature of the above-mentioned calcination temperatures.

The N,P-AC-supported nickel catalysts (Ni/N,P-AC) were also prepared by facile impregnation method. The above doped activated carbon was immersed in 0.1 $mol \cdot L^{-1}$ nickel nitrate ($Ni(NO_3)_2 \cdot 6H_2O$) solution, stirred at 30 °C for several hours, and then dried at 100 °C overnight. Afterwards, it was calcined at 400 °C in a tubular furnace under nitrogen for 4 h and subsequently reduced for another 2 h at the same temperature in a hydrogen atmosphere. Finally, the Ni/N,P-AC were obtained and marked as Ni/N,P-AC-T (T = 800 °C and 900 °C). The nickel loading of the catalysts was 20 wt-%. The 20% Ni/AC where the carbon support without heteroatomic doping was also prepared with the same preparation method for comparison.

2.3 Characterizations of catalysts

N_2 adsorption-desorption was measured at a liquid nitrogen temperature (−77 K) by using the NOVA-2200e physical adsorption instrument. The specific surface area and pore size of the samples were correspondingly calculated by the Brunauer-Emmett-Teller (BET), Barrett-Joyner-Halenda, and Horvath-Kawazoe methods. The surface elemental composition and element valence distribution were detected by X-ray photoelectron spectroscopy (XPS) on a Kratos Axis Ultra DLD spectrometer with Al Kα X-ray as the excitation source. Transmission electron microscopy (TEM) was measured on a TecnaiG2 20 ST microscope at 200 kV to observe the morphologies and detailed microstructure of Ni/NP-AC. Raman spectroscopy was employed to characterize the extent of disorder in the carbon materials and was obtained on a Lab RAM Aramis Micro-Raman spectrometer with an excitation

wavelength of 532 nm with 2 lm spot size. X-ray diffraction (XRD) measurements were conducted on a Japan RigakuD/Max 2550VB$^+$ 18 kW diffractometer (Cu Kα radiation) in the range of 2° to 90° at a scanning rate of $10° \cdot \min^{-1}$ and operated at 40 mA and 40 kV. The H_2 uptake quantity, metallic surface area, and metal dispersions were obtained by hydrogen chemisorption using a ChemBET-3000 Adsorption instrument.

2.4 Catalytic procedure

The hydrogenation of 1,5-dinitronaphthalene was carried out in a 50 mL Teflon-lined stainless steel autoclave equipped with a pressure gauge and a magnetic stirrer. Firstly, 2.0 g 1,5-dinitronbaphthale, 20 mL solvent *N*,*N*-dimethylformamide, and 0.1 g catalyst were introduced into the reactor. Then, the reactor was purged several times with N_2 to remove air, and then purged several times with H_2 to remove N_2. The reaction was subsequently run at the targeted temperature and pressure. After reaction, the reactor was depressured, and the catalyst was isolated from the reaction solution by filtering and the substances in the filtrate were identified by liquid chromatograph mass spectrometer. Furthermore, the conversion of 1,5-dinitronbaphthale and the product yields were determined by high-performance liquid chromatography.

2.5 Computational methodology

The graphene mode without any defect was introduced for simulating the original carbon support to carry out the theoretical calculation and investigate the influence of the defects on the nickel metal anchoring. All molecular modes were fully optimized using a DFT method. These modes are optimized using the dMol[3] module in the Material Studio package, using the generalized gradient approximation in the Perdew-Burke-Ernzerhof parameterization. The double numerical augmented with d-functions was chosen as the basis set. The convergence in energy, max force, and displacement were set 2×10^{-5} Ha (1 Ha = 27.2114 eV), 0.004 Ha·Å^{-1}, and 0.005 Å, respectively. The k-point grids of $2 \times 2 \times 1$ were employed for structure optimization.

The binding energy E_{bind} (Ni_n) can be used to evaluate the stability of isolated Ni_n (n = 2–6) cluster per metallic atom, which is defined as follows [31,32]:

$$E_{\text{bind}}(\text{Ni}_n) = [n \times E(\text{Ni}) - E(\text{Ni}_n)]/n, \quad (1)$$

where $E(\text{Ni}_n)$ and E(Ni) are the total energies of an isolated and a single Ni atom, respectively; and n is the number of Ni atoms in the Ni_n cluster. The larger E_{bind} (Ni_n) is, the more stable the isolated Ni_n (n = 2–6) cluster will be. Similarly, the binding energy of the Ni_n cluster on the surface of the support $E_{\text{bind}}(\text{Ni}_n/\text{Support})$ per metallic atom is given by the following equation:

$$E_{\text{bind}}(\text{Ni}_n/\text{Support}) = [n \times E(\text{Ni})] + E(\text{Support}) - E(\text{Ni}_n/\text{Support})]/n, \quad (2)$$

where $E(\text{Ni}_n/\text{Support})$ is the total energy of the supported Ni_n cluster, E(Support) is the total energy of the support. E_{bind} (Ni_n/Support) reflects the stability of the Ni_n cluster supported on the catalysts. The supports investigated in the present work include graphene, graphene with defects after removing nitrogen species, and nitrogen-doped graphene (graphite N, pyridine N, and pyrrolic N) for comparation.

Finally, the H_2 adsorption energy on the Ni supported graphene with or without phosphorus has also been calculated to demonstrate the function of phosphorus doping. The adsorption energy of H_2, which is denoted by E_{ads} (H_2), is defined as follows.

$$E_{\text{ads}}(\text{H}_2) = E(\text{Ni} + \text{Support}) + E(\text{H}_2) - E(\text{H}_2/\text{Ni} + \text{Support}), \quad (3)$$

where $E(\text{H}_2/\text{Ni} + \text{Support})$ is the total energy of H_2 on the Ni catalysts, and E(Ni + Support) is the total energy of the Ni catalysts mode with or without P.

3 Results and discussions

3.1 N,P-AC supports and Ni/N,P-AC characterization

The textural properties of the N,P-AC supports co-doped by nitrogen and phosphorus at different temperatures are shown in Table S1 (cf. Electronic Supplementary Material, ESM). As can be seen, the heteroatomic doping of N,P-AC materials possesses highly specific surface area similar to the original active carbon. Furthermore, as the calcination temperature increases, the specific surface area becomes larger and the pore volume slightly increases [8]. The element and the valence distributions of nitrogen and phosphorus on the N,P-AC supports are shown in Fig. S1 (cf. ESM). The peaks assigned to the N and P elements appeared after tuning the activated carbon with heteroatoms, indicating that IL enabled the nitrogen and phosphorus to successfully dope onto the activated carbon. Furthermore, with the increase of calcination temperatures to 900 °C, the peak of element N disappeared and the content of P decreased slightly. These results exhibit that the different element contents could be adjusted by changing the pre-treatment temperature, and the phosphorus element is more stable than nitrogen as the dopant in the active carbon materials.

Figure 1 shows the N1s and P2p XPS spectra of the support samples. It can be seen that the different nitrogen species could be detected between 396.0 and 406.0 eV in N,P-AC-800. The deconvolution of the N1s spectra exhibits four nitrogen species located at the binding

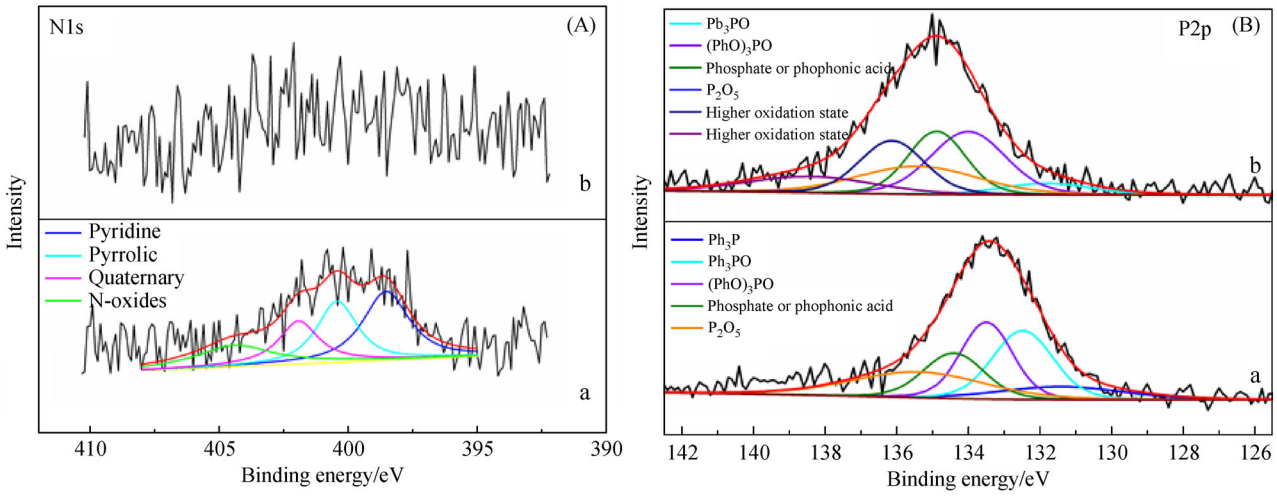

Fig. 1 (A) N 1s and (B) P 2p XPS spectra of the N,P-ACs-T: (a) N,P-AC-800 and (b) N,P-AC-900.

energies of 398.5, 399.5, 400.9 and 404.3 eV, which are assigned to pyridinic-N, pyrrolic-N, graphitic-N, and oxidized-N, respectively [22,33,34]. With the treatment temperature from 800 °C to 900 °C, the atomic content of nitrogen in the N,P-ACs decreased from 1.49% to trace (Table 1). Interestingly, the doped phosphorus species were more stable than the nitrogen species. The different phosphorus species could be detected between 128.0 and 140.0 eV, and the phosphorus peaks varied considerably with the different temperatures. Among them, peaks around 130–132 eV are correlated with the low oxidation state of phosphorus while 132.5−137 eV are associated with the high oxidation state of phosphorus [35,36]. It can be seen from Table 1 that the low oxidation state of phosphorus accounted for 11.7% on the activated carbon doped at 800 °C. With the increase of temperature, the low oxidation state disappeared and the high oxidation state of phosphorus appeared, accounting for about 33.9%. For N,P-AC-800, it possessed five ranges of binding energy peaks, of which the 131.2 eV peak is attributed to Ph_3P in the low oxidation state, the peak of 132.4 eV belongs to Ph_3PO, the peak of 133.3 eV is assigned to $(PhO)_3PO$, the peak of 134.4 eV is correlated with a phosphate or phosphonic acid, and the peak value of more than 135 eV is linked to P_2O_5 [22]. Moreover, the oxidation state of phosphorus broadens for N,P-AC-900. The two binding energy peaks of phosphorus in the higher oxidation state appear at 136.1 and 137.1 eV. According to the literatures, phosphorus in a highly-oxidized state easily loses electrons and transfers them to surrounding atoms, which is beneficial for promoting the dissociation of hydrogen [34,35,37]. From the XPS analysis results, it can be seen that the nitrogen can be mostly removed by tuning the treatment temperature and the phosphorus doping could result in abundant oxidation states of phosphorus species. The content of phosphorus and the distribution of its oxidation state could also be altered by employing different treatment temperatures.

Further structural information about the obtained N,P-ACs can be observed from Raman spectra. As shown in Fig. 2(A), two typical characteristic bands were clearly detected, in which the G band (~1596 cm^{-1}) indicates the in-plane vibration of aromatic carbon atoms, while the D band (~1340 cm^{-1}) arose from defects on the graphitic lattice of the disordered sp^3-hybridized carbon. Generally, the ratio of the D band and G band (I_D/I_G) is applied to illustrate the disorder degree of carbon materials [38]. Obviously, the I_D/I_G value of N,P-ACs is greater than pristine AC (I_D/I_G = 1.16), suggesting the presence of many defects in N,P-ACs after heteroatom doping. In addition, with a higher pyrolysis temperature, a higher I_D/I_G ratio of N,P-ACs is obtained, which may result from more defects by the elimination of nitrogen and phosphorus dopants in the carbon matrix as the temperature increases. Meanwhile, the increasing defects of the carbon material may enhance the anchoring for nickel metal by

Table 1 Nitrogen and phosphorus content and the composition on the N,P-ACs prepared at different temperatures [a)]

Sample	N/At-%	N_P/%	N_{Pyr}/%	N_Q/%	NO_x/%	P/At-%	Ph_3P/%	Ph_3PO/%	$(PhO)_3PO$/%	Phosphate/ phosphoric acid/%	P_2O_5 /%	High oxidated state P/%
N,P-AC-800	1.49	34.6	26.5	20.0	18.9	1.68	11.7	24.9	24.0	18.1	21.3	–
N,P-AC-900	–	–	–	–	–	1.47	–	9.1	16.9	23.3	16.8	33.9

a) N_P: pyridine-N, N_{Pyr}: pyrrolic-N, N_Q: graphitic-N, NO_x: N-oxides

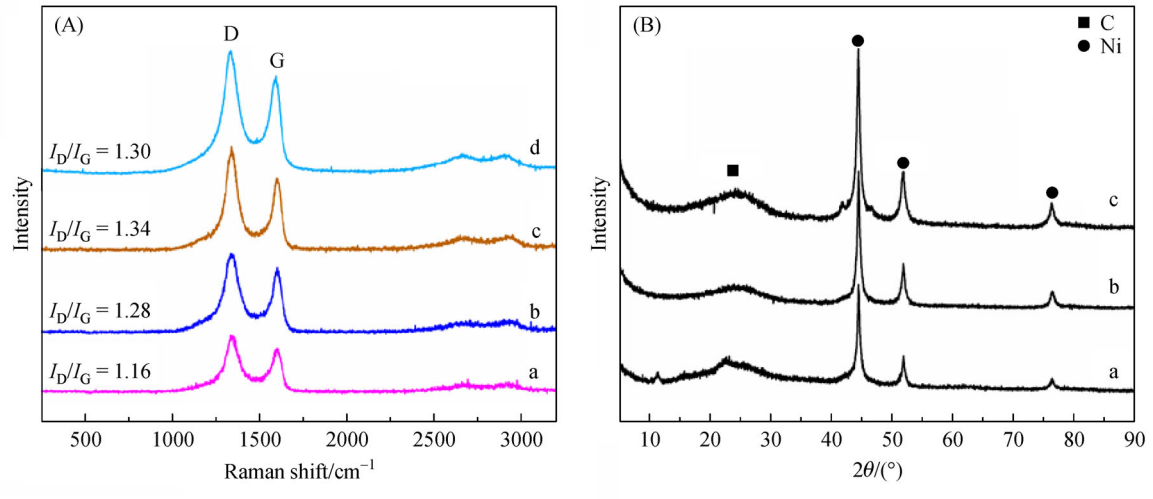

Fig. 2 (A) Raman spectra of (a) AC, (b) N,P-AC-800, (c) N,P-AC-900, and (d) Ni/N,P-AC-900; (B) XRD spectra of the catalysts (a) Ni/AC, (b) Ni/N,P-AC-900, and (c) Ni/N,P-AC-800.

improving the binding capacity of nickel metal and the N, P-ACs, leading to the even dispersion of nickel metal particles on the surface of catalysts [39]. After loading Ni on the catalysts, the supported Ni-based catalysts exhibit relatively lower I_D/I_G values than N,P-AC-900, which may be attributable to the nanoparticles preferring to anchor on the structural defect sites on the surface of N,P-AC-900 during the loading process [40].

Figure 2(B) shows the XRD patterns of Ni/N,P-AC. It can be seen that all of the samples have a broad diffraction peak around 2θ = 20°–30°, which belongs to the typical carbon structure. The diffraction peaks at 2θ = 44°, 52° and 77° are attributed to crystalline nickel [41]. After doping with IL, the spectra of Ni/N,P-AC-800 and Ni/N,P-AC-900 showed better purity than the undoped activated carbon-supported nickel catalyst.

Figure 3 shows the comparison of the TEM diagrams between Ni/N,P-ACs and Ni/AC. It can be observed that most of the nickel particles loaded on the surface of the undoped activated carbon were seriously aggregated, though it contained a higher percentage of small nickel particles, and the non-uniform particle size of nickel particles were distributed in 8–35 nm. After the heteroatomic doping in the activate carbon support, the nickel particles became larger and more uniform, which may due to the defects formed on the supports by heteroatomic doping. The existence of defects provides more anchoring sites for the nickel to load and grow, which could decrease aggregation and improve the dispersion of nickel particles. Compared with Ni/N,P-AC-800, the Ni/N,P-AC-900 catalyst shows good dispersion and larger uniform nickel particle size concentrated in the range of 18–20 nm. This may be related to the Raman results that the N,P-AC-900 support shows a larger defect degree than the N,P-AC-800, and the defect size might become larger after removing the nitrogen species with the higher treatment temperature.

As can be seen from the above characterization, the carbon surface properties can be greatly changed after it was co-doped by nitrogen and phosphorous, resulting in more anchoring sites for the loading of metal particles. After the nitrogen species were removed under a treatment temperature of 900 °C, the support could obtain more defects for nickel loading and enhance the binding capacity between the N,P-AC supports and the nickel metal, improving the stability of the nickel nanoparticles and allowing them to be more uniformly dispersed on the support. Hydrogen chemisorption was conducted to quantify the hydrogen uptake and the metallic surface area. The results are shown in Table S2 (cf. ESM). The Ni/N-AC-900, Ni/P-AC-900, and Ni/N,P-AC-T showed better hydrogen uptake, metal surface area, and metal dispersion compared with the undoped Ni/AC, Ni/N-AC-900. Particularly, the Ni/N,P-AC-900 exhibited a maximum hydrogen uptake of 157.09 $\mu L \cdot g^{-1}$, a metallic surface area of 0.55 $m^2 \cdot g^{-1}$, and a metal dispersion of 0.33%, which might facilitate the catalytic activity in the hydrogenation of aromatic nitro compounds.

3.2 Catalytic performance

As can be seen from Table 2, the target product is 1,5-diaminonaphthalene in the 1,5-dinitronaphthalene hydrogenation reaction. Other products, such as the intermediate of 5-nitro-1-naphthalenamine and hydrazonaphthylamine, were also detected [4]. Compared with the other Ni-based catalysts, Ni/N,P-AC-900 exhibited decent activity and presented 96.8% conversion of 1,5-dinitronaphthalene when the reaction time was 50 min. However, 91.5% selectivity to the intermediate 5-nitro-1-naphthalenamine was obtained compared to 7.5% selectivity to the target

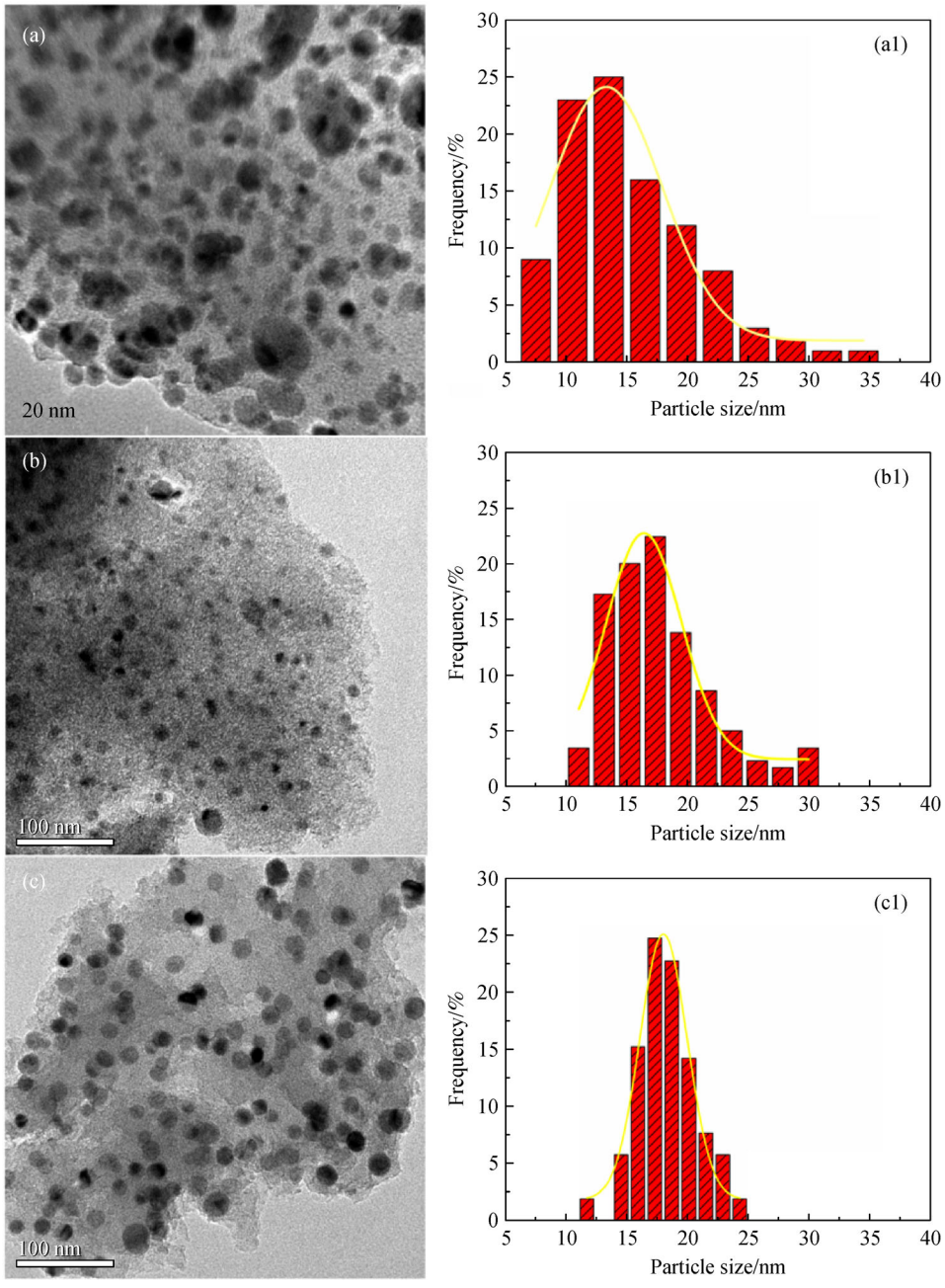

Fig. 3 TEM pictures of the (a) Ni/AC, (b) Ni/N,P-AC-800, and (c) Ni/N,P-AC-900.

1,5-diaminonaphthalene. The intermediate product 5-nitro-1-naphthalenamine could be completely converted with 95.8% selectivity to 1,5-diaminonaphthalene as the reaction time was prolonged to 150 min under the catalysis of Ni/N,P-AC-900, which is comparable to commercial Pd/C (95.9% selectivity under 50 min). For the original Ni/AC, most of the intermediate product of 5-nitro-1-naphthalenamine cannot be converted for the lower activity of the catalysts even though the reaction time was extended to 300 min. Additionally, Ni/N,P-AC-800 presented better activity than the Ni/AC, as the support was tuned by heteroatoms. The above catalytic performance results demonstrate that the heteroatomic doping on the active carbon could significantly enhance the catalytic properties in the liquid hydrogenation of 1,5-dinitronaphthalene. To explore the function of co-doped N and P, the control experiments catalyzed by Ni/N-AC-900 and Ni/P-AC-900 under the same experimental conditions were investigated. Compared with Ni/N,P-AC-900, the catalytic activities of both of the single doped catalysts were much lower. In fact, even the reaction time was 300 min, and a large quantity of intermediate 5-nitro-1-naphthalenamine could not be converted to the target product. The results also show that Ni/P-AC-900 exhibited better activity than the Ni/N-

Table 2 The catalytic performances of different samples in the liquid-phase hydrogenation of 1,5-dinitronaphthalene [a)]

Catalysts	Time/min	Conv./%	Select./%		
			5-Nitro-1-naphthalenamine	1,5-Diaminonaphthalene	Others
Ni/AC	300	100	82.4	16.2	1.4
	150	86.0	94.9	4.3	0.8
N,P-AC-900	300	–	–	–	–
Ni/N-AC-900	300	100	80.4	15.9	3.7
Ni/P-AC-900	300	100	35.2	61.8	3.0
Ni/N,P-AC-800	300	100	38.3	59.2	2.5
	150	99.5	88.8	9.6	1.9
Ni/N,P-AC-900	150	100	–	95.8	4.2
	50	96.8	91.5	7.5	1.0
5% Pd/C	50	100	–	95.9	4.1

a) Reaction conditions: 1,5-dinitronaphthalene, 2 g; DMF, 20 mL; Catalyst, 0.1 g; Temperature, 100 °C; H_2 pressure, 0.6 MPa; Ni loading content, 20%.

AC-900 under the same reaction conditions. The above catalytic performance verified that the co-doped heteroatoms on the active carbon could significantly enhance the catalytic properties. The characterization results simultaneously corroborated that the heteroatoms tuning on the active carbon can enhance the defects amounts, which will further increase after removing nitrogen species by a higher temperature treatment at 900 °C. These defects may provide good anchoring sites for nickel atom deposition by strong interactions between the heteroatom or defects and the nickel atoms. The Ni/N,P-AC-900 — with larger and extremely uniform nickel particles — exhibited the maximum hydrogen uptake, metallic surface area, and metal dispersion, allowing it remain steady in the liquid hydrogenation of 1,5-dinitronaphthalene to produce 1,5-diaminonaphthalene. The results obtained in this work are relatively better than the results in previous literatures (Table S3, cf. ESM). The recycling stability of the Ni/N,P-AC-900 has also been investigated and the results are shown in Fig. S2 (cf. ESM). It can be seen that the catalytic performance could be relatively stable in running five cycles, and the catalytic activity of the catalyst gradually decreased, which may due to the active metal leaching on the catalysts. Prolonging the reaction time could enhance the conversion and selectivity to the target product. The XRD and TEM of Ni/N,P-AC-900 after recycling were investigated and are presented in Fig. S3 (cf. ESM). It indicates that the crystallization of the nickel metal decreased and the particle size of nickel nanoparticles could be maintained around 18–20 nm after being recycled 6 times.

3.3 DFT results

The simplest carbon material graphene was chosen as the model of carbon support to calculate the nickel binding energy on the surface to simulate the deposition and growth of nickel atoms on the different tuned surfaces of carbon materials. For simulating the growth behavior of nickel atoms, the modes of Ni_n clusters (n = 2–6) were first constructed and then the binding energy was calculated, as shown in Fig. S4 (cf. ESM). The binding energy E_{bind} (Ni_n) can be used to evaluate the stability of the isolated Ni_n (n = 1–6) cluster per metallic atom. After geometry optimization, the binding energies of the Ni_n clusters and the total energy are shown in Table S4 (cf. ESM). The results indicate that the stability of the nickel atom clusters gradually increase with the increasing number of nickel atoms [31].

For comparing the binding energy of Ni particles on the different modified carbon supports, the original carbon support (without heteroatomic doping and defect), doped carbon support with nitrogen species (graphite N, pyridine N, and pyrrolic N), and carbon support with defect but without nitrogen species were constructed and geometrically optimized (Fig. S5, cf. ESM). The optimal nickel binding configurations on different supports were prejudged by the comparison of three different binding sites of nickel on top, bridge, and hollow (Fig. S6, cf. ESM). After the geometry optimization, E_{bind} (Ni/Support) was calculated by Eq. (2) and the results reflect the stability of the Ni atom supported on the surfaces of different catalysts. The total energy and E_{bind} (Ni/Support) results are presented in Table 3. It can be seen that the binding energy of Ni on the original carbon without heteroatoms or defects is lowest (~1.68 eV), while tuning the carbon support via nitrogen heteroatom doping can enhance the binding energy. Among the different nitrogen species, the binding energies between Ni and pyridine N- or pyrrolic N-doped carbon support (~5.70 eV) are much higher than the one binded on the graphite N-doped carbon support (~2.03 eV), which might due to the defects along with the doping of the former two nitrogen species. After pretreatment at 900 °C, the nitrogen species were removed and more defects were left during the Ni/N,P-AC-900 preparation. Thus, the binding energy of Ni on two kinds of defects (the 12-ring

Table 3 The binding energies of Ni on the different modes of modified carbon supports

Ni on different support modes	Total E/eV	E_{bind} (Ni)/eV
Original carbon support	−74203.2212	1.685837824
Graphite-N carbon	−74654.7350	2.033443912
Pyridine-N carbon	−73617.5047	5.704832528
Pyrrolic-N carbon	−73617.5049	5.704233864
Carbon with 12r-defect	−73164.0703	6.603644888
Carbon with 14r-defect	−72127.2686	6.872472236
2Ni on Carbon with 14r-defect	−113168.2959	5.025827819
3Ni on Carbon with 14r-defect	−154208.7550	4.220880532
4Ni on Carbon with 14r-defect	−195250.2349	4.073607147
5Ni on Carbon with 14r-defect	−236291.2345	3.889190199
6Ni on Carbon with 14r-defect	−277307.2994	−0.389540234

Table 4 The adsorption energies of H_2 on Ni loaded on the different carbon supports

Different modes	Total E/eV	E_{ads} (H_2)/eV
H_2	−31.57349582	–
Ni on carbon support without P doping (1)	−72127.20158	–
Ni on carbon support with P doping (2)	−81413.59703	–
H_2 adsorption on (1)	−72159.25703	0.48195717
H_2 adsorption on (2)	−81445.92856	0.75803652

defect and 14-ring defect) was also investigated. It indicates that the binding energy can further be improved to about 6.60 eV for the 12-ring defect and 6.87 eV for the 14-ring defect after nitrogen elimination, which explains how the carbon support with larger quantities of defects provides more anchoring sites for the nickel particle to deposit and grow into uniform particles with perfect dispersion.

To simulate the growth of the nickel clusters on the carbon support with defects, the Ni_n (n = 1–6) clusters were loaded on the mode of carbon support with the 14-ring defect (Fig. S7, cf. ESM). The binding energies between the Ni_n cluster and carbon support were also calculated using Eq. (2). The results are also shown in Table 3. It can be observed that the binding energies gradually decrease with the increasing number of nickel atoms. Compared with the binding energies of the Ni_n clusters shown in Table S4, it can be inferred that the defects on the carbon support potentially inhibited the aggregation of the nickel particles and the particle sizes may relate to the defect sizes on the carbon support.

The function of phosphorus atom doping was investigated by calculating the H_2 adsorption energies E_{ads} (H_2) on the carbon with defect-loaded Ni with or without phosphorus doping [42]. Two kinds of H_2 adsorption configurations (Top and Parallel) were compared, and the optimized adsorption modes are shown in Fig. S8 (cf. ESM). The results of E_{ads} (H_2) on the different Ni-loaded carbon materials are exhibited in Table 4. It can be seen that the adsorption energy of H_2 on the support with phosphorus doping is much larger than the one without phosphorus, demonstrating that H_2 can be more easily adsorbed and dissociated on the Ni load carbon support with phosphorus doping.

4 Conclusions

Nitrogen and phosphorus co-doped activated carbon (N,P-AC) was prepared under different temperatures, and used as the support for loading non-noble nickel metal to catalyze the hydrogenation reaction of aromatic compounds. The characterization results show that the nitrogen species were removed when the N,P-ACs were pretreated under 900 °C, and its supported nickel catalyst (Ni/N,P-AC-900) exhibited larger hydrogen uptake and highly-dispersed nickel metal. It also indicated that the nitrogen elimination could obtain more defects, which are favorable for the nickel metal anchoring on the supports. These results indicate that the heteroatomic doping on the activated carbon shows a positive effect in this liquid-phase aromatic compound hydrogenation reaction, presenting inspiring catalytic activity and selectivity. Among them, the N,P-ACs prepared under 900 °C-supported nickel (Ni/N,P-AC-900) showed extremely high catalytic activity and selectivity, with the yield of 1,5-diaminonaphthalene reaching 95.8% under 100 °C and 150 min. It exhibited relatively stable catalytic performance during the reaction. The computational study of the nickel binding energy was also conducted. It demonstrated that the defects formed by heteroatomic doping are beneficial to nickel anchoring and deposition to form highly dispersed and uniform nickel particles. The phosphorus species in combination with the defects are good for H_2 adsorption and dissociation. These findings could provide a promising route for the potential design of the aromatic compound hydrogenation catalysts to significantly decrease the cost from using noble metal catalysts in the industry.

Acknowledgements This work was supported by the National Natural Science Foundation of China (Grant No. 21908185), Project of Hunan Provincial Natural Science Foundation of China (Grant No. 2018JJ3497), Project of Hunan Provincial Education Department (Grant Nos. 19B572 and 20B547), Collaborative Innovation Center of New Chemical Technologies for Environmental Benignity and Efficient Resource Utilization, and National Department of Education Engineering Research Centre for Chemical Process Simulation and Optimization.

Electronic Supplementary Material Supplementary material is available in the online version of this article at https://doi.org/10.1007/s11705-020-1994-x and is accessible for authorized users.

References

1. Zhu G B, Yi Y H, Han Z X, Wang K. Sensitive electrochemical sensing for polycyclic aromatic amines based on a novel core-shell multiwalled carbon nanotubes@ graphene oxide nanoribbons heterostructure. Analytica Chimica Acta, 2014, 845: 30–37
2. Suraru S, Würthner F. Strategies for the synthesis of functional naphthalene diimides. Angewandte Chemie, 2014, 53(29): 7428–7448
3. Yang C H, Chen G, Zhang L. Progress of one-step oxidative amination of benzene to aniline. Speciality Petrochemicals, 2009, 26 (4): 72–76
4. Xiong W, Wang K J, Liu X W, Hao F, Xiao H Y, Liu P L, Luo H A. 1,5-Dinitronaphthalene hydrogenation to 1,5-diaminonaphthalene over carbon nanotube supported non-noble metal catalysts under mild conditions. Applied Catalysis A, General, 2016, 514: 126–134
5. Huang L, Lv Y, Wu S T, Liu P L, Xiong W, Hao F, Luo H A. Activated carbon supported bimetallic catalysts with combined catalytic effects for aromatic nitro compounds hydrogenation under mild conditions. Applied Catalysis A, General, 2019, 577: 76–85
6. Chen L, Xia K S, Huang L Z, Li L W, Pei L B, Fei S X. Facile synthesis and hydrogen storage application of nitrogen-doped carbon nanotubes with bamboo-like structure. International Journal of Hydrogen Energy, 2013, 38(8): 3297–3303
7. Prithi J A, Rajalakshmi N, Rao R G. Nitrogen doped mesoporous carbon supported Pt electrocatalyst for oxygen reduction reaction in proton exchange membrane fuel cells. International Journal of Hydrogen Energy, 2018, 43(9): 4716–4725
8. Yu X L, Nie R F, Zhang H F, Lu X H, Zhou D, Xia Q H. Ordered mesoporous N-doped carbon supported Ru for selective adsorption and hydrogenation of quinoline. Microporous and Mesoporous Materials, 2018, 256: 10–17
9. Shi X P, Yu H B, Gao S, Li X Y, Fang H H, Li R J, Li Y Y, Zhang L J, Liang X L, Yuan Y Z. Synergistic effect of nitrogen-doped carbon-nanotube-supported Cu-Fe catalyst for the synthesis of higher alcohols from syngas. Fuel, 2017, 210: 241–248
10. Zhou L N, Liu D, Li J S, Tang H L, Xie Z Z, Qu D Y. Electrochemical hydrogen storage in a nitrogen-doped uniformed microporous carbon. International Journal of Hydrogen Energy, 2018, 43: 14096–14102
11. Chang B B, Shi W W, Yin H, Zhang S R, Yang B C. Poplar catkin-derived self-templated synthesis of N-doped hierarchical porous carbon microtubes for effective CO_2 capture. Chemical Engineering Journal, 2019, 358: 1507–1518
12. Ratso S, Kruusenberg I, Käärik M, Kook M, Saar R, Pärs M, Leis J, Tammeveski K. Highly efficient nitrogen-doped carbide-derived carbon materials for oxygen reduction reaction in alkaline media. Carbon, 2017, 113: 159–169
13. Sui Z Y, Li X, Sun Z Y, Tao H C, Zhang P Y, Zhao L, Han B H. Nitrogen-doped and nanostructured carbons with high surface area for enhanced oxygen reduction reaction. Carbon, 2018, 126: 111–118
14. Yao Y J, Hu Y, Yu M J, Lian C, Gao M X, Zhang J, Li G W, Wang S B. Nitrogen-doped carbon encapsulating molybdenum carbide and nickel nanostructures loaded with PVDF membrane for hexavalent chromium reduction. Chemical Engineering Journal, 2018, 344: 535–544
15. Ruiz-García C, Heras F, Calvo L, Alonso-Morales N, Rodriguez J, Gilarranz M. Platinum and N-doped carbon nanostructures as catalysts in hydrodechlorination reactions. Applied Catalysis B: Environmental, 2018, 238: 609–617
16. Wang Z K, Han W F, Tang H D, Li Y, Liu H Z. Preparation of N-doped ordered mesoporous carbon and catalytic performance for the pyrolysis of 1-chloro-1,1-difluoroethane to vinylidene fluoride. Microporous and Mesoporous Materials, 2019, 275: 200–206
17. Liu L Z, Zeng G, Chen J X, Bi L L, Dai L M, Wen Z H. N-Doped porous carbon nanosheets as pH-universal ORR electrocatalyst in various fuel cell devices. Nano Energy, 2018, 49: 393–402
18. Li G, Yi Q F, Yang X K, Chen Y, Zhou X L, Xie G. Ni-Co-N doped honeycomb carbon nano-composites as cathodic catalysts of membrane-less direct alcohol fuel cell. Carbon, 2018, 140: 557–568
19. Zhang T F, Xia Q X, Wan Z X, Yun J, Wang Q M, Kim K. Highly porous carbon nanofoams synthesized from gas-phase plasma for symmetric supercapacitors. Chemical Engineering Journal, 2019, 360: 1310–1319
20. Guo D D, Xin R R, Zhang Z, Jiang W, Hu G S, Fan M H. N-Doped hierarchically micro- and mesoporous carbons with superior performance in supercapacitors. Electrochimica Acta, 2018, 291: 103–113
21. Panomsuwan G, Saito N, Ishizaki T. Nitrogen-doped carbon nanoparticle-carbon nanofiber composite as an efficient metal-free cathode catalyst for oxygen reduction reaction. ACS Applied Materials & Interfaces, 2016, 8(11): 6962–6971
22. Cao Y H, Yu H, Tan J, Peng F, Wang H J, Li J, Zheng W X, Wong N B. Nitrogen-, phosphorous- and boron-doped carbon nanotubes as catalysts for the aerobic oxidation of cyclohexane. Carbon, 2013, 57: 433–442
23. Xu X, Tang M H, Li M M, Li H R, Wang Y. Hydrogenation of benzoic acid and derivatives over Pd nanoparticles supported on N-doped carbon derived from glucosamine hydrochloride. ACS Catalysis, 2014, 4(9): 3132–3135
24. Gong W B, Chen C, Zhang H M, Zhang Y, Zhang Y X, Wang G Z, Zhao H J. Highly selective liquid-phase hydrogenation of furfural over N-doped carbon supported metallic nickel catalyst under mild conditions. Journal of Molecular Catalysis A Chemical, 2017, 429: 51–59
25. Tang D H, Sun X, Zhao D, Zhu J J, Zhang W T, Xu X L, Zhao Z. Nitrogen-doped carbon xerogels supporting palladium nanoparticles for selective hydrogenation reactions: the role of pyridine nitrogen species. ChemCatChem, 2018, 10(6): 1291–1299
26. Wang S G, Zhou P, Jiang L, Zhang Z H, Deng K J, Zhang Y H, Zhao Y X, Li J J, Bottle S, Zhu H Y. Selective deoxygenation of carbonyl groups at room temperature and atmospheric hydrogen pressure over nitrogen-doped carbon supported Pd catalyst. Journal of Catalysis, 2018, 368: 207–216
27. Cao Y L, Mao S J, Li M M, Chen Y Q, Wang Y. Metal/porous carbon composites for heterogeneous catalysis: old catalysts with improved performance promoted by N-doping. ACS Catalysis, 2017, 7(12): 8090–8112
28. Kim D P, Lin C L, Mihalisin T, Heiney P, Labes M M. Electronic properties of nitrogen-doped graphite flakes. Chemistry of Materi-

als, 1991, 3(4): 686–692

29. Yang W, Yang W, Kong L N, Song A L, Qin X J, Shao G J. Phosphorus-doped 3D hierarchical porous carbon for high-performance supercapacitors: a balanced strategy for pore structure and chemical composition. Carbon, 2018, 127: 557–567
30. Patiño J, López-Salas N, Gutiérrez M C, Carriazo D, Ferrer M L, Monte F. Phosphorus-doped carbo-carbon nanotube hierarchical monoliths as true three-dimensional electrodes in supercapacitor cells. Journal of Materials Chemistry. A, Materials for Energy and Sustainability, 2016, 4(4): 1251–1263
31. Li J R, Zhang R G, Wang B J. Influence of the hydroxylation of γ-Al_2O_3 surfaces on the stability and growth of Cu for Cu/γ-Al_2O_3 catalyst: a DFT study. Applied Surface Science, 2013, 270: 728–736
32. Xiong W, Wang Z N, He S L, Hao F, Yang Y Z, Lv Y, Zhang W B, Liu P L, Luo H A. Nitrogen-doped carbon nanotubes as a highly active metal-free catalyst for nitrobenzene hydrogenation. Applied Catalysis B: Environmental, 2020, 260: 118105–118114
33. Hulicova-Jurcakova D, Kodama M, Shiraishi S, Hatori H, Zhu Z, Lu G Q. Nitrogen-enriched nonporous carbon electrodes with extraordinary supercapacitance. Advanced Functional Materials, 2009, 19(11): 1800–1809
34. Hasegawa G, Deguchi T, Kanamori K, Kobayashi Y, Kageyama H, Abe T, Nakanishi K. High-level doping of nitrogen, phosphorus, and sulfur into activated carbon monoliths and their electrochemical capacitances. Chemistry of Materials, 2015, 27(13): 4703–4712
35. Imamura R, Matsui K, Takeda S, Ozaki J, Oya A. A new role for phosphorus in graphitization of phenolic resin. Carbon, 1999, 37: 261–267
36. Paraknowitsch J P, Zhang Y J, Wienert B, Thomas A. Nitrogen- and phosphorus-co-doped carbons with tunable enhanced surface areas promoted by the doping additives. Chemical Communications, 2013, 49(12): 1208–1210
37. Paraknowitsch J P, Thomas A. Doping carbons beyond nitrogen: an overview of advanced heteroatom doped carbons with boron, sulphur and phosphorus for energy applications. Energy & Environmental Science, 2013, 6(10): 2839–2855
38. Jiang H, Wang Y Q, Hao J Y, Liu Y S, Li W Z, Li J. N and P co-functionalized three-dimensional porous carbon networks as efficient metal-free electrocatalysts for oxygen reduction reaction. Carbon, 2017, 122: 64–73
39. Chen M, Shao L L, Guo Y X, Cao X Q. Nitrogen and phosphorus co-doped carbon nanosheets as efficient counter electrodes of dye-sensitized solar cells. Chemical Engineering Journal, 2016, 304: 303–312
40. Lv Y, Cui H S, Liu P L, Hao F, Xiong W, Luo H A. Functionalized multi-walled carbon nanotubes supported Ni-based catalysts for adiponitrile selective hydrogenation to 6-aminohexanenitrile and 1,6-hexanediamine: switching selectivity with [Bmim]OH. Journal of Catalysis, 2019, 372: 330–351
41. Gong W B, Chen C, Zhang H M, Zhang Y, Zhang Y X, Wang G Z, Zhao H J. Highly selective liquid-phase hydrogenation of furfural over N-doped carbon supported metallic nickel catalyst under mild conditions. Journal of Molecular Catalysis A Chemical, 2017, 429: 51–59
42. Ao Z M, Peeters F M. Electric field activated hydrogen dissociative adsorption to nitrogen-doped graphene. Journal of Physical Chemistry C, 2010, 114(34): 14503–14509